The System ZrO_2–CaO Studied by the Electron Spin Resonance of Mn^{2+} Ions

G. BACQUET, J. DUGAS,* AND C. ESCRIBE†

Laboratoire de Physique des Solides (associé au C.N.R.S.), Université Paul Sabatier, 118, rte de Narbonne, 31077 Toulouse Cédex, France

AND A. ROUANET

Laboratoire des Ultra-Réfractaires du C.N.R.S., Odeillo, 66120 Font-Romeu, France

We have used the electron spin resonance of Mn^{2+} ions to study the zirconia–calcia system from 9 to 60 mole % CaO. With the exception of single crystals of calcia-stabilized zirconia (CSZ) with 15 and 20 mole % CaO, the experiments were carried out on polycrystalline samples. From the different values measured for the hyperfine coupling constant A with increasing amount of calcia, we have deduced that Mn^{2+} substitutes for Ca^{2+} in the three following host lattices: cubic CSZ, $CaZrO_3$, and CaO.

1. Introduction

There are three well-defined polymorphs of pure zirconia (ZrO_2), namely, the monoclinic, tetragonal, and cubic structures. The monoclinic phase the accurate structure of which was first reported by McCullough and Trueblood (*1*) is stable up to about 1000°C and then transforms over a 100°C range to the tetragonal phase. Both structures are related to the fluorite structure. Finally the compound takes the cubic CaF_2 structure above 2300°C as quoted initially by Smith and Cline (*2*). A recent review article was devoted to the martensitic transformation in zirconia (*3*).

Since the monoclinic to tetragonal phase transformation is associated with a volume change, pure zirconia is unsatisfactory as a ceramic. However, at high temperatures, the addition of variable amounts of some MO or

* Present address: Departement de Physique, Université Mohamed V, Rabat, Maroc.

† Present address: I.L.L., B.P. 156, 38042 Grenoble Cédex, France.

M_2O_3 (M = metal) oxides enables one to obtain stable cubic solid solutions (*4*). For instance, the phase diagrams of the system CaO–ZrO_2, as determined by high-temperature X-ray diffraction and differential thermal analysis (DTA), indicate that a cubic phase with CaF_2 structure (calcia-stabilized zirconia, CSZ) exists over a range of compositions from 8 to 20 mole % CaO (*5–7*).

By neutron diffraction studies of single-crystal and polycrystalline specimens of CSZ, Carter and Roth (*8*) have found that the oxygen polyhedra of the cubic phase are considerably distorted from those of CaF_2 when CSZ is quickly cooled from above 1200°C. They also showed by long annealing experiments (1080 hr for single crystals) that CSZ undergoes an ordering transformation near 1000°C which can be reversed by heating for a short time at 1400°C. Figure 1 shows an extension to four molecules of the model they proposed for the ordered structure. Among the four possible substitutional sites, the A, B, and C sites, which can be deduced one from
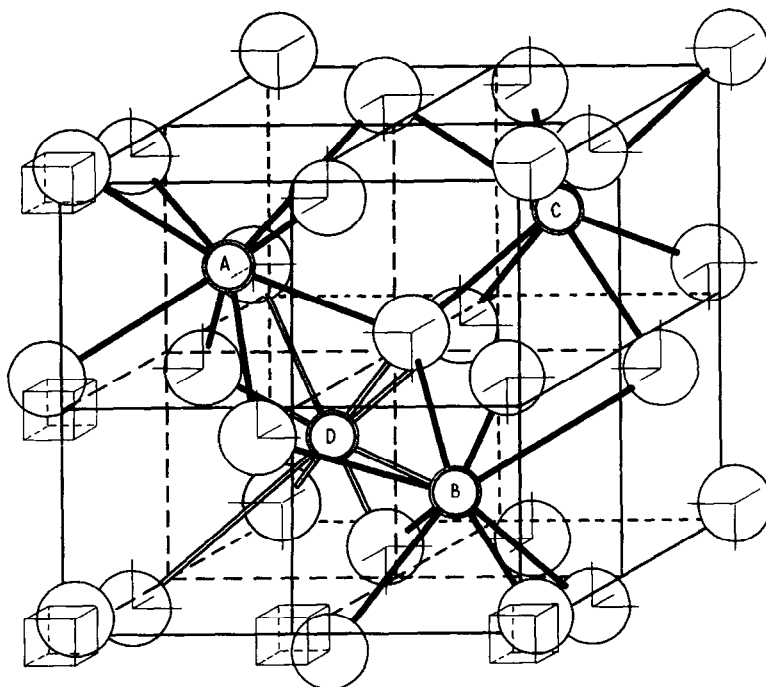
FIG. 1. Ordered arrangement of O^{2-} ions in CSZ as seen by Carter and Roth (8), showing the four possible substitutional sites.

another by $\pm 2\pi/3$ rotations about $\langle 111 \rangle$ directions, belong to the D_{2d} symmetry point group. The D site has a particular configuration consisting of two imbricate tetrahedra having the same C_2-axis, and belongs to the T_d point group.

Our previous results on Gd^{3+}- or Yb^{3+}-doped single crystal CSZ supported the conclusion of Carter and Roth concerning the disorder–order transformation and the ordered arrangement (9). Effectively, we recorded ESR spectra characteristic of a weak axial symmetry along each of the three $\langle 100 \rangle$ directions, and we could assert consequently that the oxygen vacancies needed to preserve the charge balance are not in nearest neighbor sites with respect to both used trivalent impurities ions.[1] These spectra were attributed to paramagnetic ions substituted in the A, B, and C sites. We thought these impurity ions

[1] The dissociation of the O^{2-} vacancy M^{3+} ion complexes (with $M = Gd$ and Fe) was also found in the case of M^{3+}-doped single-crystal monoclinic zirconia (10).

avoided the D site where four O^{2-} ions move in, because their sizes (Gd^{3+}, 0.97 Å; Yb^{3+}, 0.86 Å) are more important than the Zr^{4+} one (0.79 Å).

To check whether this behavior of impurity ions in calcia–zirconia system was general, we undertook a series of experiments using Mn^{2+} as a dopant. This ion, of which the radius is 0.80 Å, has an electronic configuration of $3d^5$ with a ground state of $^6S_{5/2}$, which is an orbital singlet. The existence of a nuclear spin $I = \frac{5}{2}$ leads to a hyperfine interaction between the nuclear and electron spins. In the spin hamiltonian, describing the ESR spectra, this interaction is characterized by a term $\mathbf{S} \cdot \bar{A} \cdot \mathbf{I}$, where $\bar{A}$ is the hyperfine coupling tensor. The value of the isotropic part A of this interaction depends generally on the number n of ligands in the $(Mn-X_n)$ cluster and upon the character of the $Mn-X$ bond (ionic or covalent).

According to the nature and the strength of the crystal field, the ESR spectra of Mn^{2+} in single-crystal host lattices consist of five groups

of six hyperfine lines (axial field) or of six pentads (cubic field). With powdered samples only the six "allowed" ($\Delta m_I = 0$) hyperfine lines (and sometimes three doublets of $\Delta m_I = 1$ "forbidden" lines) of the $m_s = -\frac{1}{2} \to \frac{1}{2}$ fine structure transition are observed.

The above considerations explain why Mn^{2+} was chosen as a dopant.

2. Samples

2a. Single-Crystal Specimens

Two different compositions in calcia were used in the starting powders: 15 mole% and 22 mole%. The specimens were obtained from the Laboratoire d'Electrochimie des Solides at Grenoble (France), where they were prepared using a Travelling Zone Melting technique described in (11). The amount of calcia along the growth axis was checked by means of electron microanalysis, and a more or less important gradient of calcia was found according to the length of the obtained single crystal and to the quantity of CaO in the starting powder (12).

In the case of $(ZrO_2)_{0.85}$–$(CaO)_{0.15}$ (hereafter referred to as CSZ 15) we could isolate crystals of about 6 to 10 mm^3, doped with about 3000 ppm of Mn^{2+}. We used Laüe technique to select the specimens the pattern of which exhibited the smallest spots characteristic of the f.c.c. phase. Because it is impossible to cleave CSZ, the samples used during this work were oriented by the same technique and subsequently polished to make it possible to have the Zeeman field vector rotated in a (110) plane.

When the amount of calcia was equal to 22 mole% (or 20 mole%) in the starting powder it was almost impossible to obtain a good crystallization of the product. The maximum volume of the crystallites, which had a thin needle shape, was lower than 2 mm^3. All but one gave poor Laüe diagrams. Due to its small size, the sample we used, hereafter referred to as CSZ 20, could not be oriented correctly. We shall see later that this was not important at all.

2b. Polycrystalline Samples

We also used solid solutions of zirconia–calcia doped with about 1000 ppm of MnO,

where the amount of CaO was included between 9 and 30 mole% and also equal to 60 mole%. The samples were made by melting of the constituent oxides, mixed in convenient proportions, by means of a solar furnace of the Laboratoire des Ultra-Réfractaires at Odeillo (France).

Powdered samples of Mn^{2+}-doped calcium zirconate (CaZrO$_3$) were prepared by different methods: (1) melting as above followed by (a) slow cooling (sample Ia); (b) quenching in water (sample Ib); (c) splat cooling (sample Ic); (2) mixing of ZrO$_2$ and CaCO$_3$ in molecular proportions followed by a firing at 1400°C for 48 hr (sample II).

3. Results

The ESR spectra were recorded at room temperature with a homemade X-band spectrometer using homodyne detection and a 100-kHz field modulation, the rectangular resonator cavity operating in the TE$_{102}$ mode.

3a. Single-Crystal Specimens

As grown specimens of CSZ 15 gave a resolved spectrum superimposed to about a 500 G broad unresolved line. This last was attributed to aggregated Mn^{2+} ions. As shown in Fig. 2, which corresponds to the magnetic field parallel to a $\langle 100 \rangle$ direction, the resolved spectrum exhibits more than 30 lines. It is interesting to note here the existence of such a spectrum with this amount of calcia. To try to improve this ESR signal some crystals were annealed at 1000°C for a few days. The result was a decrease of its intensity, whereas in the case of Gd^{3+}- and Yb^{3+}-doped CSZ 14 resolved spectra appeared under annealing (9).

As in the case of the two quoted rare-earth impurities, the Mn^{2+} spectrum of Fig. 2 was interpreted as being a consequence of the superposition of three 30 line spectra: one *parallel* and two (identical) *perpendicular* (Fig. 3). Each of them is due to Mn^{2+} ions in sites of essentially cubic symmetry, with an extra-weak axial distortion along one of the three cube edges. The spectra are called parallel or perpendicular when the direction of the distortion is either parallel or perpendicular to the static field. These three defects
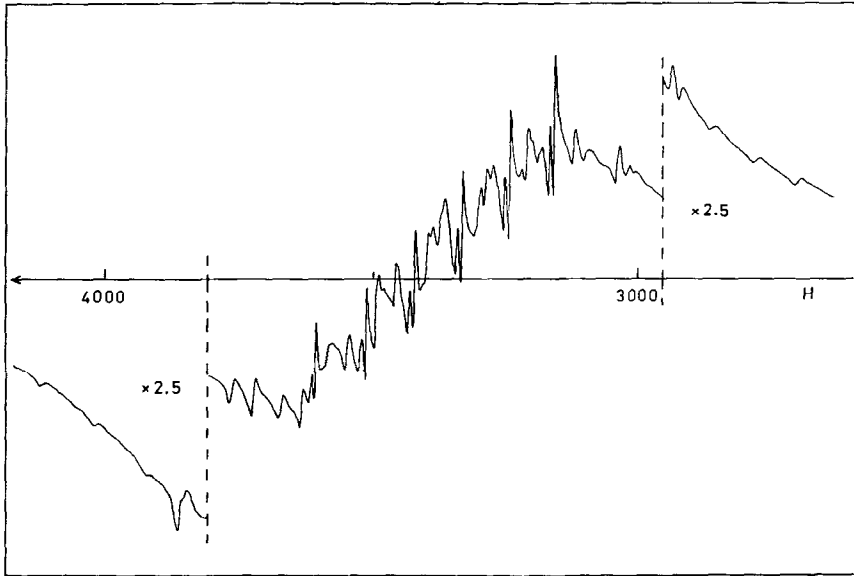
FIG. 2. ESR spectrum of Mn^{2+} in CSZ 15: The magnetic field is aligned along a $\langle 100 \rangle$ direction.
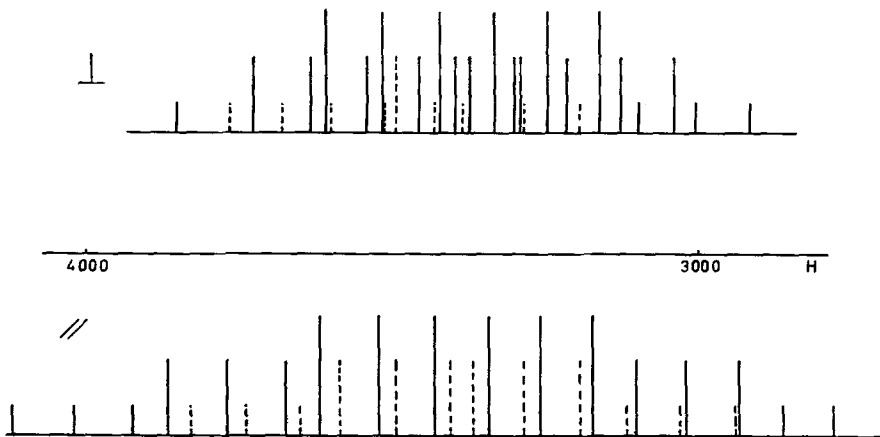

FIG. 3. Relative line positions for the perpendicular and the parallel spectra with $H//\langle 100 \rangle$. The line intensities are not to scale. The dashed lines are not resolved.

are magnetically equivalent when the magnetic field is parallel to a $\langle 111 \rangle$ direction which we verified.

It was impossible to follow each individual line during the angular variation in a (110) plane owing to their important overlapping and the appearance of so-called *forbidden* hyperfine lines as soon as the magnetic field is not parallel to a $\langle 100 \rangle$ direction.

The ESR pattern given in Fig. 2 was fitted to a spin hamiltonian:

$$\mathcal{H} = g\mu_B H \cdot S_z + \mathbf{S} \cdot \bar{A} \cdot \mathbf{I} + \sum_{m=0,2} B_2{}^m O_2{}^m$$

$$+ \sum_{m=0,2,4} B_4{}^m O_4{}^m, \qquad (1)$$

where the $O_n{}^m$ are the Stevens' operator equivalents.

To find the constants corresponding to the parallel and perpendicular cases we used the formulas given by Hutchings (13) concerning the rotation of Stevens' operator equivalents.

The spin hamiltonian was written down as

$$\mathcal{H} = \mathcal{H}_0 + \mathcal{H}_p, \qquad (2)$$

where $\mathcal{H}_0$ is the Zeeman term and

$$\mathcal{H}_p = \sum_{m=0,2} B_2{}^m O_2{}^m + \sum_{m=0,2,4} B_4{}^m O_4{}^m$$
$$+ AS_z I_z + (B/2)(S_+ I_- + S_- I_+). \qquad (3)$$

Using perturbation theory up to second order we obtained thus the equations giving the energy differences which were identical to hv for two levels in which the "allowed" transitions ($\Delta m_s = 1$; $\Delta m_I = 0$) take place.

The g factor as well as the hyperfine splitting constant were found to be isotropic and, within the experimental uncertainty, no rhombic deformation was evident. On the other hand, as is often the case with Mn^{2+} ion, the contribution of the fourth-order terms of the crystal field is very weak. Particularly it

TABLE I

SPIN HAMILTONIAN PARAMETERS OF Mn^{2+} IN CSZ 15 AND COMPARISON BETWEEN EXPERIMENTAL AND THEORETICAL LINE POSITIONS

Spin-Hamiltonian parameters	Parallel spectrum		Perpendicular spectrum	
	Observed (G)	Calculated (G)	Observed (G)	Calculated (G)
$g = 1.9990 \pm 0.0005$	2687	2694	2914	2919
$A = (-83.3 \pm 0.4) \times 10^{-4}$ cm^{-1}	2770	2774	3006	3008
$B_2{}^0 = (-38.0 \pm 0.2) \times 10^{-4}$ cm^{-1}	2855	2856	3040	3040
$B_4{}^0 = (-9 \pm 0.2) \times 10^{-7}$ cm^{-1}	2935	2938	unresolved	3100
$B_2{}^2 = (0 \pm 0.3) \times 10^{-4}$ cm^{-1}	unresolved	2940	3127	3127
	3019	3020	3164	3164
	unresolved	3027	3195	3194
	3103	3104	3217	3216
	unresolved	3117	3250	3249
	3172	3173	unresolved	3290
	unresolved	3191	3294	3294
	3258	3258	3305	3307
	unresolved	3280	3336	3336
	3345	3344	3377	3376
	unresolved	3370	unresolved	3389
	unresolved	3408	3402	3401
	3434	3433	3425	3425
	unresolved	3495	unresolved	3436
	3524	3525	3461	3461
	unresolved	3584	unresolved	3497
	3620	3619	unresolved	3515
	unresolved	3652	3516	3516
	3678	3676	3547	3548
	unresolved	3741	unresolved	3598
	3770	3770	3612	3610
	unresolved	3833	3638	3637
	3865	3866	unresolved	3682
	3923	3924	3729	3729
	4019	4023	3767	3769
	4118	4122	3854	3858

was impossible to obtain the $B_4{}^2$ and $B_4{}^4$ terms because the overlap of some lines which may be up to 10 G wide (14). Nevertheless, with the constants, the sign of which was determined by reference to that of A (negative), and which are quoted in Table I, the calculated line positions fit the measured ones with a precision better than 0.3%.

With the unique specimen of Mn^{2+}-doped CSZ 20 that we could use we recorded an isotropic six-line spectrum centered on $g = 2.0008 \pm 0.0005$. The signal intensity was too weak for us to see the expected doublets of "forbidden" hyperfine lines (see 3b in this paper). From the center of the spectrum to the wings, the line intensity decreases and the line width increases. Lowering the temperature to LNT a splitting of the two outer lines was observed, but with a very poor resolution. Within the experimental error this splitting did not depend on the orientation of the crystal in the dc field.

The value of the hyperfine coupling constant was found to be $A = -76.85 \times 10^{-4}$ cm^{-1}. Comparison with some other oxides doped with either Mn^{2+} or Mn^{4+} is given in Table II, from which it is clear that no information about the valence state of manganese can be obtained from the A value.

TABLE II

HYPERFINE COUPLING CONSTANT VALUE FOR Mn^{2+} AND Mn^{4+} IN SOME OXIDES

Oxide	Valence state	$\|A\|$ ($\times 10^{-4}$ cm^{-1})	Reference
MgO	2	81.0	(15)
	4	70.8	(16)
CaO	2	80.8	(17)
	4	73.0	(18)
SrO	2	80.5	(19)
	4	75.0	(19)
CaZrO$_3$[a]	2	80.6	(20)
	4	73.0	(20)
TiO$_2$	4	mean value 70	(21)
CSZ 20[a]	?	76.85	this work

[a] See the discussion.

The probable existence of a strong disorder of the anion sublattice explains the non-observation of the fine structure transitions other than $m_s = -\frac{1}{2} \rightarrow \frac{1}{2}$.

After long annealing (1000 hr) at various temperatures of CSZ 20 single crystals, Michel (22) observed by X-ray diffraction, two ordered phases called Φ_2 and Φ_1, respectively. The first appears when the annealing temperature is in the 1050–1350°C range. All these observed interferences could be interpreted by assuming a rhombic cell the parameters of which are $a = 12.1$ Å, $\alpha = 97°55'$. This cell could have the composition $Ca_{10}Zr_{40}O_{90}\square_{10}$, where $\square$ represents an O^{2-} vacancy. The structure of the ϕ_1 phase, which is obtained at temperature lower than 1050°C, seems to be related to the ϕ_2 one and could correspond to a lower symmetry.

Starting from these results our crystal was annealed at 1000°C for 1 week first, then up to 1 month. No change was observed on the spectrum and consequently no answer could be given concerning the manganese neighborhood.

As it was not easy to obtain good single-crystal specimens of CSZ with variable amount of calcia, we realized polycrystalline samples as indicated above.

3b. Polycrystalline Samples

Using the polycrystalline samples whose amount of calcia varied from 9 to 16 mole%, we recorded a unique spectrum which looks like that obtained with single-crystal CSZ 15 when $H /\!/ \langle 111 \rangle$. The hyperfine coupling constant value is -83.3×10^{-4} cm^{-1}.

Between 16 and 19 mole% CaO the ESR spectrum is the superposition of two different patterns. The first is identical to the former one, and its intensity decreases with the increasing amount of calcia. The reverse holds true for the second which corresponds to an A value equal to -76.85×10^{-4} cm^{-1}.

Above 19 mole% CaO up to 30 mole%, we observed the spectrum represented in Fig. 4 which is that observed with single-crystal CSZ 20, but with a stronger intensity. Three doublets of "forbidden" hyperfine lines are resolved, and this will permit us to determine the valence state of manganese.
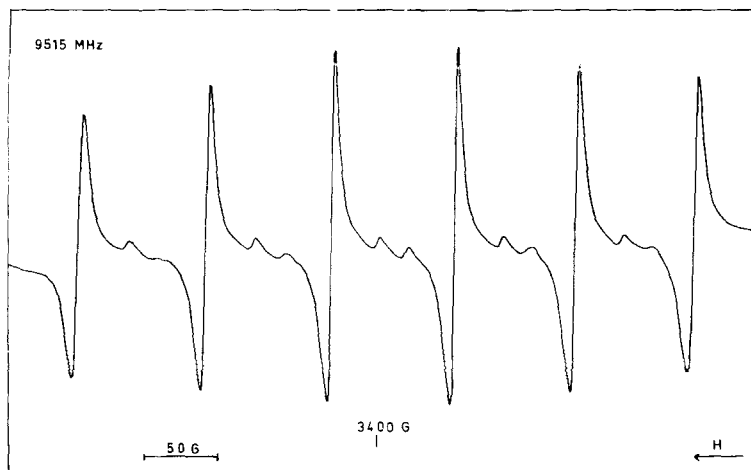
FIG. 4. ESR spectrum in melted ZrO₂–CaO solid solutions when the amount of calcia is included between 19 mole % (CSZ) and 50 mole % (CaZrO₃).

This spectrum can be described by a spin hamiltonian:

$$\mathscr{H} = g\mu_B H \cdot S_z + A \cdot \mathbf{I} \cdot \mathbf{S} + D\{S_z^2 - \tfrac{1}{3}S(S+1)\} - g_N\mu_N \mathbf{H} \cdot \mathbf{I}. \qquad (4)$$

As we shall see later, we can obtain an evaluation of the $D = 3B_2{}^0$ value from the forbidden line intensity.

The fine structure splitting having an identical effect on each of the six hyperfine lines, the magnitude of A and g were determined from measurements of the difference between the center position of adjacent lines (m_I and $m_I - 1$). Such differences are given to third order by

$$\Delta H(m_I) = -\left(A' - \frac{15A'^3}{4H_0{}^2}\right) + \frac{A'^2}{2H_0}(2m_I - 1), \qquad (5)$$

where $H_0 = h\nu/g\mu_B$ and $A' = A/g\mu_B$ with ν the constant microwave frequency. The g and A values so obtained are

$$g = 2.0008 \pm 0.0005 \quad \text{and}$$
$$A = -76.85 \times 10^{-4} \text{ cm}^{-1}.$$

We can observe the forbidden transitions because the off-diagonal terms are nonzero. Expressions derived from perturbation theory for the magnetic field at which resonances occur involve the electronic spin quantum

number S explicitly. Wolga and Tseng (23) have given expressions for the differences between adjacent forbidden lines to third order in perturbation theory.

As shown in Table III, the experimental field differences agree very well with the theoretical ones deduced from the formula:

$$\Delta H_f(m_I) = -\frac{25A'^3}{2H_0{}^2}(2m_I - 1) + \frac{17A'^2}{2H_0} + 2g_N H_0 \qquad (6)$$

corresponding to $S = \tfrac{5}{2}$.

The comparison when $S = \tfrac{3}{2}$ is very poor: We can then conclude that the observed spectrum is due to Mn²⁺.

From the intensity of the forbidden lines we can estimate the value of the axial field

TABLE III

FORBIDDEN DOUBLET SPLITTING
AS A FUNCTION OF m_I

m_I	Observed (G)	Calculated (G)
$\tfrac{3}{2}$	20.6	20.8
$\tfrac{1}{2}$	19.5	19.4
$-\tfrac{1}{2}$	18.4	18.7

parameter D. To do this estimation we used the formula

$$R = \left(\frac{3D}{4g\mu_B H_0}\right)^2 \sin^2 2\theta \left[1 + \frac{S(S+1)}{3m_s(m_s-1)}\right]$$
$$\times [I(I+1) - m_I^2 + m_I] \qquad (7)$$

given by Bleaney and Rubins (24) for the relative intensity of a first-order forbidden transition to an allowed one, where the latter is of the type $(m_s, m_I) \to (m_s - 1, m_I)$ and the former is $(m_s, m_I - 1) \to (m_s - 1, m_I)$, for instance.

The averaged angular term of Eq. (7) equals $\frac{8}{15}$, and with $m_s = m_I = \frac{1}{2}$ and $R = 0.33$ we found $3B_2{}^0 = D \cong 32.7 \times 10^{-4}$ cm^{-1} which could explain the line width variation with the increasing magnetic field (8.8; 5.8; 3.9; 4.9; 6.4; 7.3; in gauss). The corresponding $B_2{}^0$ value is about four times lower than that found in the case of CSZ 15.

A special attention was devoted to calcium zirconate $CaZrO_3$ which has a distorted perovskite structure at room temperature (25–27). In the case of specimens Ia, Ib, and Ic (see 2b) we obtained the same spectrum as above, the corresponding hyperfine coupling constant value of which is -76.85×10^{-4} cm^{-1}. These samples were then annealed in air at 1200°C for 5 hr, but the spectra recorded before and immediately after heat treatment were identical.

The spectrum observed in the case of non melted samples (II) is shown in Fig. 5. It is compounded of two different six-line spectra of almost equal intensity. The first corresponds to $A = -76.85 \times 10^{-4}$ cm^{-1} (Sp. 1). The second (Sp. 2), for which $A = -80.8 \times 10^{-4}$ cm^{-1} is analogous to that reported by Henderson (20) who used solid polycrystalline samples of $CaZrO_3$ prepared by cold pressing of calcium and zirconium oxides in molecular proportions, followed by firing at 1450°C and sintering at 1800°C in vacuum. After annealing in air at 1200–1300°C his samples then exhibited a weak spectrum, the intensity of which decayed to zero intensity within a few hours at room temperature. The corresponding A value (-73×10^{-4} cm^{-1}) was typical for the Mn^{4+} ion. Such a spectrum was not observed with sample II immediately after an annealing at 1200°C for 15 hours. Nevertheless, with respect to the spectrum of Fig. 5 (which was recorded before heat treatment), a minor modification appeared: Sp. 2 was twice as intense as Sp. 1.

With melted samples of Mn^{2+}-doped $(ZrO_2)_{0.40}$ $(CaO)_{0.60}$ we only obtained a six principal line pattern which corresponds to $A = -80.8 \times 10^{-4}$ cm^{-1} (Sp. 2). Its intensity is
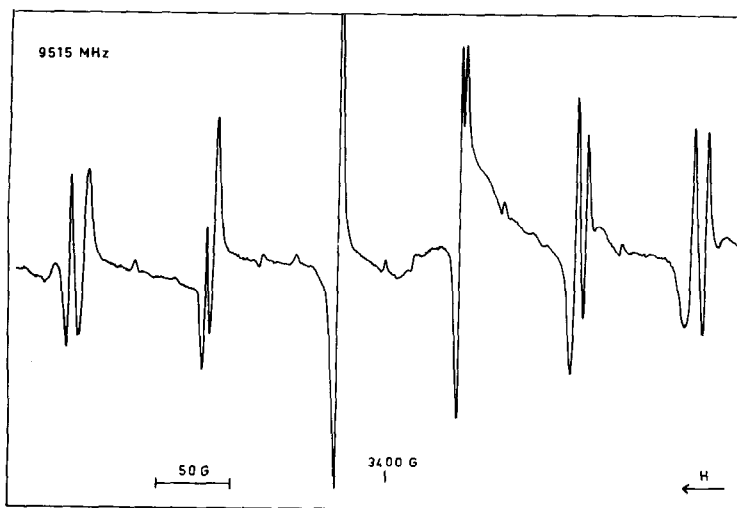

9515 MHz

50 G

3400 G

H

FIG. 5. ESR pattern recorded with nonmelted $CaZrO_3$.

such that the five doublets of forbidden hyperfine lines $(\Delta m_I = 1)$ are easily observed.

4. Discussion and Conclusions

With single crystals of CSZ as well as with polycrystalline samples of zirconia–calcia solid solutions we observed some changes in the hyperfine coupling constant value A of Mn^{2+} with the amount of calcia. For this paramagnetic ion, Šimanek and Müller (28) have shown that the A value depends mainly on the covalency C of the Mn–X bond (X is the ligand) and on the number n of ligands: A decreases almost linearly as C/n increases. The differences in A values of CSZ having different amounts of calcia can be explained by assuming a different coordination number of the MnO_n cluster.

The phase diagrams of the ZrO_2–CaO system, which were determined by high temperature X-ray diffraction and Differential Thermal Analysis, have shown the existence of various compounds in the obtained solid solutions. As an example, and because the major part of our specimens were prepared using the same technique (melting by means of a solar furnace, but followed by a more or less rapid quenching) we present in Fig. 6 the results of Traverse and Foex (5).

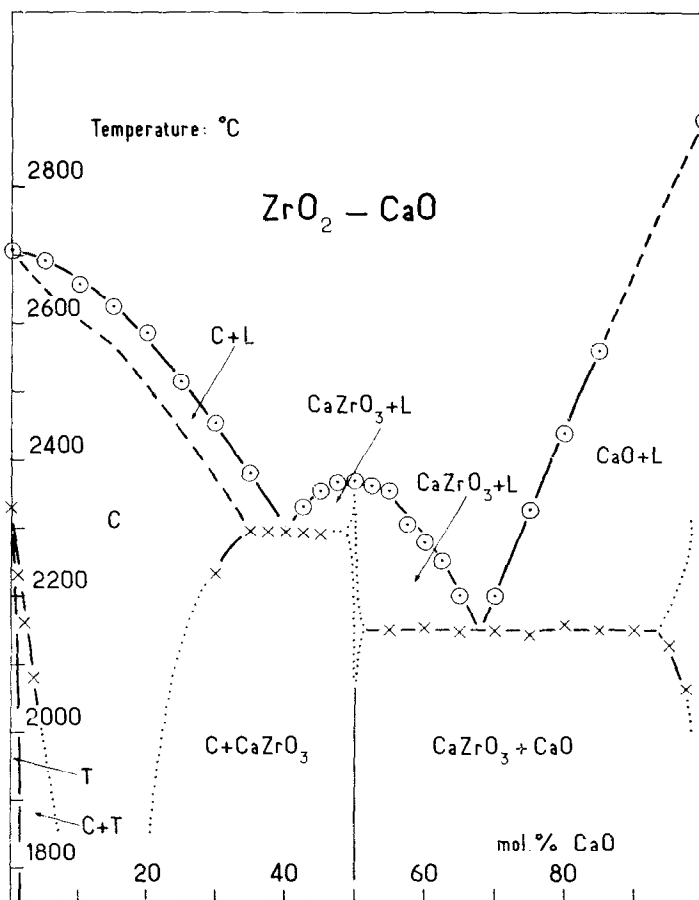Let us first focus our attention on the cubic phase (CSZ) which exists in the range 8–20

FIG. 6. Phase diagram of the ZrO_2–CaO system as seen by Traverse and Foex (5).

mole % CaO and on the results we obtained with single crystals. In CSZ 15, Mn^{2+} ions were found in sites corresponding to a weak axial symmetry along each of the three $\langle 100 \rangle$ directions, in agreement with the model proposed by Carter and Roth (8) for the *ordered* structure of CSZ. On the other hand there is no O^{2-} vacancy in the nearest neighbor position (no axial symmetry along $\langle 111 \rangle$ direction). Since the A values found in polycrystalline ThO_2 and CeO_2 were -87.5×10^{-4} and -86.2×10^{-4} cm^{-1}, respectively (29), the value of -83.3×10^{-4} cm^{-1} corresponds to a slightly distorted eightfold coordination. With CSZ 20 the value -76.85×10^{-4} cm^{-1} seems to correspond to a slightly distorted cluster (MnO_6) as the A values found at $290°K$ in the case of alkaline-earth oxides are close to -81×10^{-4} cm^{-1} (15, 17, 19). This would mean that Mn^{2+} ions would then have two O^{2-} vacancies in nearest neighbor position and that a consequent rearrangement of the anions would take place. Such a supposition did not seem reasonable.

With melted polycrystalline samples we saw that the axial spectrum ($A = -83.3 \times 10^{-4}$ cm^{-1}) decreased to zero-intensity from 16 to 19 mole % CaO, and that the spectrum (Sp. 1) corresponding to -76.85×10^{-4} cm^{-1} started to appear for 16 mole % CaO. Its intensity increased from 16 mole % CaO (CSZ 16) to 50 mole % CaO ($CaZrO_3$). A logical explanation to these two last observations can be given assuming the existence in the 8–20 mole % CaO range of some microdomains of calcium zirconate in which the Mn^{2+} ions go preferentially. As the sensitivity of the ESR technique is much higher than that of X-ray diffraction, such microdomains are detected from 16 mole % CaO.

But we saw in 3b that with nonmelted $CaZrO_3$ samples, Henderson (20) observed a spectrum which differs from that we obtained on melted samples by the linewidth value (<0.7 G) and the A value (-80.6×10^{-4} cm^{-1}). To explain this discrepancy let us consider the $CaZrO_3$ structure. At room temperature this compound would be orthorhombic according Tilloca and Perez y Jorba (25) with $a = 5.587 Å$, $b = 5.758$ Å, and $c = 8.008$ Å, or pseudo-monoclinic after Megaw (26) or Nadler and Fitzsimmons (27) the parameters being $a = c = 4.003$ Å, $b = 3.997$ Å, and $\beta = 91°43'$. Both models correspond to a strong distortion of the perovskite-type cubic structure. On the other hand Foex et al. (30) showed that above 1600°C calcium zirconate takes the cubic perovskite structure, this transformation being reversible however. Since the assumption that Mn^{2+} would be in the same site in the two $CaZrO_3$ polymorphs must be ruled out, is it possible to explain these conflicting results assuming the existence of two different substitutional sites (Ca or Zr)? This would seem logical referring to the fact that the ESR pattern we recorded with a nonmelted sample is compounded of two six-line spectra. Henderson's conclusion, based upon the instability at room temperature of the Mn^{4+} spectrum obtained after annealing, is that Mn^{2+} substitutes for Ca^{2+}. Thus the spectrum corresponding to $A = -76.85 \times 10^{-4}$ cm^{-1} (Sp. 1) might be attributed to Mn^{2+} ions located in Zr^{4+} sites. In this case a Mn^{4+} spectrum appearing after heat treatment would be very stable. We said that we did not observe such an ESR diagram. Our observations on Mn^{2+}-doped $(ZrO_2)_{0.4}(CaO)_{0.6}$ solid solutions (we found also $A = -80.8 \times 10^{-4}$ cm^{-1} in this case) added to the previous remark prove that Henderson's deduction is erroneous. Within the experimental uncertainty, the value -80.6×10^{-4} cm^{-1} is identical to that found by Shuskus (17) for Mn^{2+} in CaO (see Table II). Consequently, we think that Henderson's samples contained a weak amount of calcia ($\lesssim 2$ mole %) which could not be detected by X-ray diffraction, thus the spectrum he recorded is not due to Mn^{2+} in $CaZrO_3$ but is the $CaO:Mn^{2+}$ one. Therefore we can assert that Sp. 1 corresponds to Mn^{2+} substituted for Ca^{2+} in calcium zirconate. The distortion of the substitutional site is such that only six O^{2-} ions (in the pure perovskite structure Ca^{2+} has 12 nearest neighbors) must be included in the cluster $(Mn-O_n)$ if we refer to the A value.

Our general conclusion is that in zirconia-calcia solid solutions (from 9 mole % CaO), Mn^{2+} ions, present as impurities (~ 1000 ppm), preferentially substitute for divalent

calciums as soon as possible in the following host lattices:

(1) Cubic CSZ (fluorite type structure), where Mn^{2+} is surrounded by eight oxygens in sites of D_{2d} symmetry, the complex Mn^{2+}–O^{2-} vacancy being dissociated.

(2) CaZrO$_3$ (a deviation from perovskite structure) where only six oxygens among the strongly distorted arrangement of 12 nearest neighbors, are taken into account.

(3) CaO (cubic structure) in which Mn^{2+} is sixfold coordinated like in MnO.

References

1. J. D. MacCullough and K. N. Trueblood, *Acta Crystallogr.* **12**, 507 (1959).
2. D. K. Smith and C. F. Cline, *J. Amer. Ceram. Soc.* **45**, 249 (1962).
3. E. C. Subbarao, H. S. Maiti, and K. K. Srivastava, *Phys. Status Solidi (a)* **21**, 9 (1974).
4. H. J. Stöcker, Thesis, University of Paris (1960).
5. J. P. Traverse and M. Foex, *High Temp. High Pressures* **1**, 409 (1969).
6. R. C. Garvie, in "High Temperatures Oxides," (A. M. Alper, Ed.), part II, p. 118, Academic Press, New York (1970).
7. D. Michel, Thesis, Univerity of Paris (1967).
8. R. E. Carter and W. L. Roth, in "Electromotive Force Measurements in High Temperatures Systems," p. 125, Institute of Mining and Metallurgy Publishers, London (1967).
9. G. Bacquet, J. Dugas, C. Escribe and F. Fabre, *J. Phys. C* **6**, 1432 (1973).
10. G. Bacquet, J. Dugas, C. Escribe, J. M. Gaite and J. Michoulier, *J. Phys. C* **7**, 1551 (1974).
11. C. Deportes, B. Lorang, and G. Vitter, *Rev. Hautes Temp. Refract.* **2**, 159 (1965).
12. F. Fabre, Thesis, University of Toulouse III (1974).
13. M. T. Hutchings, "Solid State Physics," Vol. 16, p. 227, Academic Press, New York (1964).
14. A preliminary report of this observation has been made at the Vth International Conference on Magnetic Resonance, Bombay (India) (1974), G. Bacquet, J. Dugas, and C. Escribe, unpublished.
15. W. Low, *Phys. Rev.* **105**, 793 (1957).
16. B. Henderson and T. P. P. Hall, *Proc. Phys. Soc.* **90**, 511 (1967).
17. A. J. Shuskus, *Phys. Rev.* **127**, 1529 (1962).
18. B. Henderson and H. T. Tohver, *Phys. Status Solidi (a)* **51**, 761 (1972).
19. L. S. Sochava, Yu. N. Tolparov, and N. N, Kovalev, *Sov. Phys. Solid State* **16**, 205 (1974).
20. B. Henderson, *Proc. Phys. Soc.* **92**, 1064 (1967).
21. H. G. Andreson, *Phys. Rev.* **120**, 1606 (1960).
22. D. Michel, *Mat. Res. Bull.* **8**, 943 (1973).
23. G. J. Wolga and R. Tseng, *Phys. Rev.* **133A**, 1563 (1964).
24. B. Bleaney and R. S. Rubins, *Proc. Phys. Soc.* **77**, 103 (1963).
25. G. Tilloca and M. Perez y Jorba, *Rev. Int. Hautes Temp. Refract.* **1**, 331 (1964).
26. H. D. Megaw, *Proc. Phys. Soc. London* **58**, 133 (1946).
27. M. R. Nadler and E. S. Fitzsimmons, *J. Amer. Ceram. Soc.* **38**, 214 (1955).
28. E. Šimanek and K. A. Müller, *J. Phys. Chem. Solids* **31**, 1027 (1970).
29. Unpublished results.
30. M. Foex, J. P. Traverse, and J. Coutures, *C.R. Acad. Sci.* **264C**, 1837 (1967).